Journal of Catalysis 285 (2012) 74–82

Contents lists available at SciVerse ScienceDirect

Journal of Catalysis

journal homepage: www.elsevier.com/locate/jcat

Pt promotional effects on Pd–Pt alloy catalysts for hydrogen peroxide synthesis directly from hydrogen and oxygen

Jing Xu, Like Ouyang, Guo-Jin Da, Qian-Qian Song, Xue-Jing Yang, Yi-Fan Han *

State Key Laboratory of Chemical Engineering, East China University of Science and Technology, Shanghai 200237, People's Republic of China

ARTICLE INFO

Article history:
Received 13 June 2011
Revised 13 September 2011
Accepted 14 September 2011
Available online 22 October 2011

Keywords:
Pd–Pt alloy
Hydrogen peroxide synthesis
XPS
XRD
In situ DRIFT
O_2-TPD
H_2-TPD

ABSTRACT

H_2O_2 synthesis directly from H_2 and O_2 over supported Pd–Pt alloy catalysts was carried out using a semibatch reactor under ambient conditions. As compared to pure Pd, the performance of Pd–Pt catalysts was enhanced significantly. The promotional role of Pt was studied systematically by using in situ diffuse reflectance infrared Fourier transform spectroscopy of CO adsorption (DRIFTS), quantitative powder X-ray diffraction (XRD), X-rays photoelectron spectroscopy (XPS), and temperature-programmed desorption of H_2/O_2 (H_2/O_2-TPD). The spectra of DRIFT, XPS, and XRD demonstrate the formation of Pd–Pt alloy particles, which surfaces are enriched by Pt accompanying with possible electron transfer from Pd to Pt. The addition of Pt into Pd phase was proposed to impact on reactants adsorption, stabilization of intermediates such as $OOH^{\cdot}$ and $OH^{\cdot}$ radicals, and the formation and decomposition of H_2O_2.

1. Introduction

The demand for hydrogen peroxide (H_2O_2) has been increasing during the last years [1,2]. H_2O_2, as a "green oxidant," is produced mainly by a circuitous process involving the redox of alkylanthroquinone and hydroquinone intermediates [3]. However, there are several drawbacks in the current process, including slow degradation of expensive anthraquinone, gradually deactivation toward hydrogenation, and high capital costs [3]. For environmental and economic concerns, there is a renewed interest for replacing this process with a direct process, by which H_2 and O_2 are reacted directly on suitable catalysts.

Up to date, the direct process operated under ambient conditions has been studied for several decades [2,4]. For practical application, it is imperative to develop novel catalysts that can enhance both the yield and the selectivity toward H_2O_2 [5–7]. Unfortunately, most of the reported catalysts fail to meet this criterion owing to the complexity of this reaction system, except for supported Pd or Pd-alloyed catalysts with a second metal such as Au, Ag, and Pt. In particular, supported Pd–Au alloy catalysts have proved excellent performance for this reaction [8–15]. The Hutchings' group has reported the performance of Pd–Au nanoalloys supported on different metal oxides such as TiO_2, Fe_2O_3, and ZrO_2, and acidified carbon using a batch reactor system (275 K, 4.0–9.0 MPa) [16–18]. One of our studies has also demonstrated the promotional effects of Au on SiO_2 supported Pd–Au alloy catalysts using a continuous reactor system under ambient conditions [13]. However, up to now, the promotional effects of Pt on Pd–Pt alloy catalysts have rarely been reported for this reaction, even though the performances of those catalysts are close to that of Pd–Au alloy catalysts. The deep insights into the mechanism are still unavailable because the whole reaction involves three phases: solid catalysts, gaseous reagents, and liquid medium [4,19–23]. In addition, Pd–Pt alloys, as an interesting catalytic system, have also shown excellent performance for other reactions such as oxygen reduction, hydrogenation of aromatic hydrocarbons in fuel, and methane combustion [10,24–29].

In this study, supported Pd–Pt alloy catalysts with different Pd/Pt ratios were prepared by conventional incipient wetness impregnation. Fumed silica was used as the support, which is chemically inert and does not interact electronically with Pd and Pt, thus will simplify the study by ruling out the potential strong metal–support interactions. H_2O_2 synthesis was performed by using a tri-phase semibatch reactor under ambient conditions, which, in principle, will greatly reduce the risk of explosion that is caused by H_2–O_2 mixtures in the explosive regime. The catalyst structure was characterized using multi-techniques such as quantitative powder X-ray diffraction (XRD), X-ray photoelectron spectroscopy (XPS), in situ diffuse reflectance infrared Fourier transform spectroscopy of CO adsorption (DRIFTS), and temperature-programmed desorption of H_2 and O_2 (H_2- and O_2-TPD).

* Corresponding author. Fax: +86 21 64251928.
E-mail address: yifanhan@ecust.edu.cn (Y.-F. Han).

0021-9517/$ - see front matter © 2011 Elsevier Inc. All rights reserved.
doi:10.1016/j.jcat.2011.09.017

The modifications of the Pd surface upon alloying with Pt and the structure–reactivity relationship of Pd–Pt alloy catalysts for the formation and decomposition of H_2O_2 were rationalized on the basis of those results. This work aims at the understanding of H_2O_2 synthesis on Pd alloy catalysts and rational design of Pd–Pt or other bimetallic or/and alloy catalysts intended for this or other applications.

2. Experimental

2.1. Catalyst preparation and reactivity measurements

All catalysts were prepared by conventional incipient wetness impregnation using aqueous solution of $PdCl_4^{2-}$ and $PtCl_6^-$, which followed a reported method with a minor modification [30]. Palladium and Platinum were introduced into the system as Pd of 3.3 wt.% with varying the Pt content in a range 0.32–3.2 wt.%, corresponding to Pd/Pt molar ratios from 20 to 2. Pd–Pt alloys were supported on fumed silica having a Brunauer–Emmett–Teller (BET) surface area of 230 $m^2\ g^{-1}$. Prior to the reaction, the precursors were pretreated in O_2 at 673 K and then reduced in H_2 at 573 K with a flow rate of 20 mL min^{-1} for 30 min. For comparison, references such as Pd–Au alloy (Au sources from $AuCl_4^-$, Pd/Au = 4 (molar ratio)) [13], pure Pd, and pure Pt catalysts were also prepared following the same procedure.

All reactions were carried out under ambient conditions using a micro-tri-phase semibatch reactor, which is similar to the apparatus given in Ref. [5]. The reagent gases were introduced into the reactor via a fine glass frit, and the slurry containing the catalyst was stirred so as to minimize diffusion limitations. The reactor was connected to a gas chromatograph (Shimadzu GC-2014), so that the concentration of H_2 exiting the reactor could be periodically determined. Improved accuracy in H_2 analysis was achieved by using a H_2/N_2 mixture that contained 10% N_2. The concentration of H_2O_2 was analyzed colorimetrically using a UV–vis spectrophotometer (Epp2000, StellarNet Inc.) after complexation with a $TiOSO_4/H_2SO_4$ reagent. H_2O_2 selectivity, $S_{H_2O_2}$, was determined from the rate of H_2O_2 formation and the rate of H_2 conversion using Eq. (1)

$$S_{H_2O_2} = \frac{\text{Rate of } H_2O_2 \text{ formation (mole/min)}}{\text{Rate of } H_2 \text{ conversion (mole/min)}} \times 100 \quad (1)$$

In the reaction, a 4:1 O_2/H_2 gas mixture with a flow rate of 50 mL/min was introduced into the reaction system at 283 K if without any special statement. The liquid phase composed of 90 mL of ethanol or water that had been acidified with 10 mL of aqueous HCl solution to give 100 mL of liquid having the desired acid normality. Thus, the "ethanol solution" contained 10 mL of water in addition to the small amount of water that was formed during the reaction. The solutions were 0.12 M in HCl unless stated otherwise. Following each experiment, residual Pd that had deposited on the frit was removed by filling the reactor with a 1.0 M HCl solution and passing pure O_2 through it. In most cases, a yellow-orange color solution, resulting from $PdCl_4^{2-}$, was observed. In addition, in order to investigate the Pt effects on H_2O_2 decomposition, the experiments were implemented under the same reaction conditions by fixing the initial H_2O_2 concentration of 1.0 wt.% with a H_2 flow rate of 15 mL min^{-1}.

Since the 4:1 O_2/H_2 gas mixture is still in the explosive regime, care must be taken to avoid contact of the gas mixture with a dry catalyst. This was achieved first by mixing 50 mg of the catalyst with 10 mL of the solution, and then, the slurry was added back into the solution that remained in the reactor. It should be noted that with ethanol as the liquid phase, the catalyst remained wet, even in the upper regions of the reactor. Expect for a trace amount of Pd (3 ppm in solution), almost no Pt and Au elements were leached from the catalyst surface to liquid as analyzed by an Inductively Coupled Plasma (ICP) analyzer.

2.2. Characterization

2.2.1. XRD

Powder X-ray diffraction patterns were accumulated with a Bruker D8 diffractometer using Cu K(α) radiation with a step size of 0.02° two-theta (2θ) over the range 30–120°, while intensive scanning was implemented in the range 30–50° and 80–84°, respectively. Approximately 10 wt.% of standard CaF_2 (NIST 640a, a = 5.4633 Å) was mixed with catalysts to allow the precise determination of lattice constants. The whole pattern was analyzed using the Rietveld method as implemented in TOPAS-V2 with Pd and Pt [31] employed as crystallographic starting models. The lattice constant of the CaF_2 standard was fixed, and the zero shift and scale factor were optimized. The isothermal vibration parameters of all phases were fixed at 1.0 $Å^2$.

2.2.2. XPS

XPS analysis was performed on a VG ESCALAB 250 spectrometer, using Al Kα radiation (1486.6 eV, pass energy 20.0 eV). The base pressure of the instrument is about 1×10^{-9} Torr. The background contribution B (E) (obtained by the Shirley method) caused by inelastic process was subtracted, while the curve fitting was performed with a Gaussian–Lorentzian profile by a standard software. The binding energies (BEs) over the supported catalysts were calibrated by using the Si_{2p} peak at 103.5 eV and C_{1s} peak at 285.0 eV as references. The instrument was also calibrated by using Au wire (Au $4f_{7/2}$ at 84.0 eV). XPS spectra were recorded at θ = 90° of X-ray sources. The Pd/Pt molar ratios were calculated through Eq. (2) [32]:

$$\frac{N_{Pd}}{N_{Pt}} = \frac{I_{Pd}/S_{Pd}}{I_{Pt}/S_{Pt}} \quad (2)$$

where the I_{Pd} and I_{Pt} are the time-normalized intensities of the Pd_{3d} and Pt_{4f} levels, and S_{Pd} (4.642 for Pd_{3d}) and S_{Pt} (4.674 for Pt_{4f}) are the atomic sensitivity factors for X-ray sources at 90°.

2.2.3. TEM

The measurements were performed on a Tecnai TF 20 S-twin with Lorentz lens. The catalyst was first ultrasonically suspended in ethanol, and then, one drop of this slurry was deposited on a carbon-coated copper grid. The liquid phase was evaporated before the grid was loaded into the microscope. The metal particle size was estimated on the basis of 300 particles.

2.2.4. In situ DRIFT spectra of CO adsorption

CO adsorption on the fresh catalysts (pretreated in O_2 at 673 K and H_2 at 573 K with a flow rate of 20 mL min^{-1} for 30 min) was conducted in a reaction cell (modified Harricks model HV-DR2) in order to allow gas flowing continuously through the catalyst bed (ca. 0.1 g) during spectra acquisition. The spectra were recorded on a PerkinElmer FT-IR spectrum 100 (resolution: 4 cm^{-1}) spectrometer at room temperature. All infrared data were evaluated in Kubelka–Munk units, which are linearly related to the absorber concentration in spectral. Contributions from gas-phase CO were eliminated by subtracting the corresponding spectra from the pure support material.

2.2.5. H_2- and O_2-TPD

The TPD experiments were performed with a micro-fixed-bed reactor (quartz reactor with 20 cm long and 0.4 cm diameter) connected to a GC–QMS (HPR-20, Hiden Analytical Ltd.), where masses of m/e 2(H_2), 15(CH_4), 18(H_2O), 28(N_2), 32(O_2), 44(CO_2) were

monitored. Prior to adsorption, the catalyst was pretreated in O_2 at 673 K and reduced in H_2 at 573 K with a flow rate of 20 mL min^{-1} for 30 min, then cooling down in pure N_2. Adsorbents of H_2 or O_2 (20 mL min^{-1}, 30 min) were introduced into the system at 283 K. Then, the system was purged with N_2 (50 mL min^{-1}, 10 min). The temperature ramped from 283 to 853 K with a rate of 20 K min^{-1} in N_2 (50 mL min^{-1}).

3. Results

The crystalline phases of Pd–Pt alloys were analyzed by XRD (Fig. 1). For all fresh samples, reflections attributable to ⟨1 1 1⟩ ($2\theta = 40.1°$ (Pd) and 39.7° (Pt)) and ⟨2 0 0⟩ ($2\theta = 46.6°$ (Pd) and 46.2° (Pt)) face-centered cubic structures were presented with their positions adjusted according to composition (Fig. 1A). The formation of single phase alloys was identified from $Pd_{20}Pt_1$ to Pd_8Pt_1 while the peak ⟨1 1 1⟩ shifted down by Δ0.1°. With continuously increasing the Pt content to Pd_4Pt_1, a two-phase alloy was produced as evidenced by the ⟨1 1 1⟩ plane at 39.7° (Pt-rich alloy) and 40.1° (Pd-rich alloy) that were really differential by lattice constants (Table 1). The alloy structures were further demonstrated by the downshift of the reflection ⟨3 1 1⟩ from 82.2° (pure Pd) to 82.0° ($Pd_{20}Pt_1$) (Fig. 1B). On the other hand, the reflection Pt ⟨3 1 1⟩ was observed clearly for Pd_4Pt_1, Pd_2Pt_1, and pure Pt, indicating the formation of a separated Pt-rich alloy in those samples.

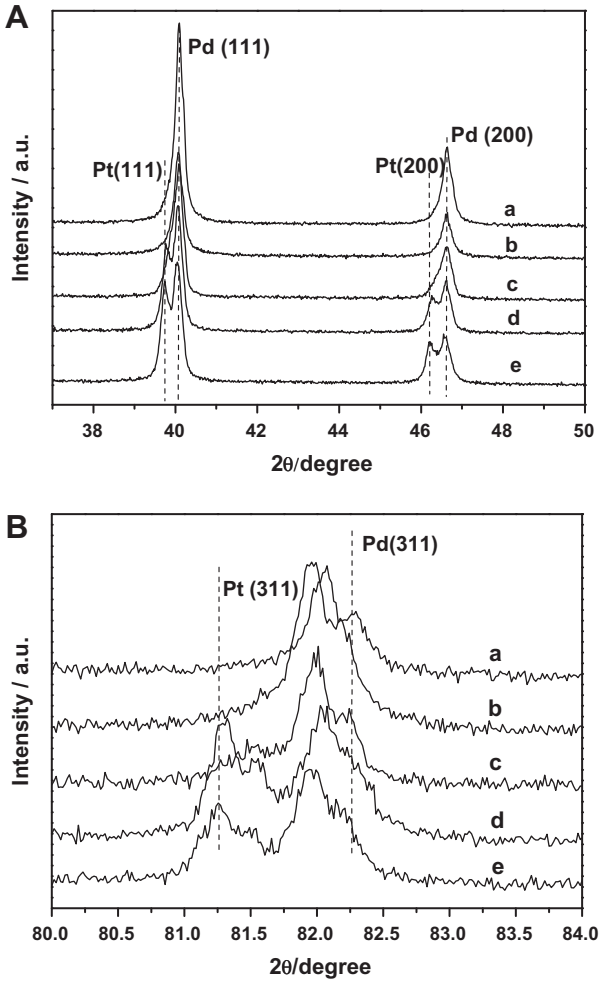

Fig. 1. (A) XRD diffraction patterns of Pd–Pt alloy catalysts in the 2θ range 35–50°; (B) in the 2θ range 80–84°. (a) $Pd_{20}Pt_1$, (b) $Pd_{16}Pt_1$, (c) Pd_8Pt_1, (d) Pd_4Pt_1, (e) Pd_2Pt_1.

High-resolution TEM images (Fig. 2a–c) show that the size distributions are almost unchanged for fresh pure Pd, $Pd_{20}Pt_1$, and $Pd_{16}Pt_1$, an average diameter of 3.5 ± 0.2 nm can be estimated. A typical size distribution curve for $Pd_{16}Pt_1$ was outlined in Fig. 2c. However, the rapid growth in particle size could be observed with further increasing the Pt content (Table 1), the average diameter of 5.0 ± 0.3 nm for Pd_8Pt_1 (Fig. 2d), 10.0 ± 0.2 nm for Pd_4Pt_1 (Fig. 2e), and 30.0 ± 0.5 nm for Pd_2Pt_1 (Fig. 2f) were determined. In addition, a high-resolution TEM image for $Pd_{16}Pt_1$ (Fig. 2c) showed one-dimensional lattice fringes of the Pd(1 1 1) lattice plane. Meanwhile, spherical particles were found for the samples from pure Pd to Pd_8Pt_1, but irregularly shaped particles were observed for Pd_4Pt_1 and Pd_2Pt_1.

The chemical states of the surface Pd and Pt atoms were analyzed using XPS. The core levels of Pd $3d_{5/2}$ at 335. 1 eV (Fig. 3A) and Pt $4f_{7/2}$ at 71.0 eV (Fig. 3B) attributing to metallic states remained unchanged upon alloying. It seems difficult to determine the electronic interaction between Pd and Pt even though charge transfer of 0.1 e from Pd to Pt in Pd–Pt alloy due to the relative high electron affinity of Pt was predicted by theoretic studies [33–35]. In addition, the Pd/Pt atomic ratios determined by XPS (Table 1) indicated that all alloy surfaces were enriched by Pt atoms because of Pt relative large electronegativity compared to Pd (the Pauling electronegativities of Pt and Pd are 2.28 and 2.20, respectively) [33].

Fig. 4 shows in situ DRIFT spectra recorded with the adsorption of CO on pure metals and Pt–Pd alloy catalysts. Linear and bridging species with maxima at 2096, 1994, and 1966 cm^{-1} were observed for pure Pd, attributing to CO adsorbed on metallic Pd atoms (Pd^0–CO) [36,37]. Upon alloying with Pt, a linear band at 2111 cm^{-1} appeared for $Pd_{20}Pt_1$ and $Pd_{16}Pt_1$, probably corresponding to linear Pd–CO complexes that lead to a remarkable loss in d-orbital electron density due to charge transfer from Pd to Pt [38] and became the dominant band for Pd_8Pt_1, Pd_4Pt_1, and Pd_2Pt_1. Meanwhile, the bridging bands decreased drastically and disappeared completely for the last three samples. The changes in vibration indicated that the Pd surface structure was significantly modified by Pt atoms. The same phenomenon was observed for a bimetallic Pt–Pd/NaY zeolite catalyst [38]. Moreover, the CO–Pt linear band (2062 cm^{-1}) [39] observed for pure Pt disappeared after alloying with Pd.

The H_2-TPD spectra (Fig. 5) show two peaks centered at 392 and 681 K for pure Pd and Pd–Pt alloy samples. The first peak is close to the one at 340 K observed for a polycrystalline Pd, associating with the multiple states of hydrogen on the Pd surface [40]. The second peak may result from the decomposition of the surface OH groups, which was also identified for a Pt/γ-Al_2O_3 catalyst [37]. The desorption amount of H_2 decreased from 106 (pure Pd) to 4(Pd_2Pt_1) μmol g_{cat}^{-1} (Table 1), and the second peak shifted down to 651 K; meanwhile, the first peak decreased gradually with increasing the Pt content and disappeared completely for Pd_2Pt_1.

The desorption amount of O_2 decreased from 60 (pure Pd) to 2 μmol g_{cat}^{-1} (Pd_2Pt_1) (Table 1), this trend is similar to that for H_2-TPD. Three peaks at 394, 496, and 653 K were detected for pure Pd but the last one diminished upon alloying with Pt (Fig. 6). The first two peaks may be attributed to the weakly adsorbed oxygen at different Pd sites, and the last peak probably originated from the decomposition of 2D palladium oxide, which has proven a precursor in the formation of PdO [41]. Presumably, the Pd–O bond strength was weakened by neighboring Pt atoms, thus led to the disappearance of the peak at 653 K.

As listed in Table 1, the activity order for all catalysts can be displayed as $Pd_{16}Pt_1 > Pd_{20}Pt_1 > Pd_8Pt_1 > Pd > Pd_4Pt_1 > Pd_2Pt_1 \gg Pt$. Pure Pd showed a middle activity, while pure Pt has no activity toward H_2O_2 synthesis but complete oxidization of H_2 to H_2O. This fact is evident that the formation of H_2O_2 occurs primarily on Pd

Table 1
The structural information and the performance of fresh SiO_2 supported Pd and Pd–Pt/Au alloy catalysts in the H_2O_2 synthesis directly from H_2 and O_2.[a]

Catalysts[b]	Particle size[c] (nm)	Surface composition (mole ratio Pd/Pt)	Cell constant a[e] (Å)		Desorption amount of H_2 ($\mu mol/g_{cat}$)	Desorption amount of O_2 ($\mu mol/g_{cat}$)	Reaction rate (mol/h g_{Pd})	H_2O_2 (wt.%)	Selectivity (%)
			Pd-rich phase	Pt-rich phase					
Pure Pd	3.8	–	3.8896		106	60	0.99	0.34	12
$Pd_{20}Pt_1$	3.5	16/1	3.8901	–	42	21	1.64	0.56	70
$Pd_{16}Pt_1$	3.6	12/1	3.8917	–	22	19	1.77	0.60	63
Pd_8Pt_1	5.0	6/1	3.8935	3.9035	7	11	1.62	0.55	52
Pd_4Pt_1	10.0	2.5/1	3.8948	3.9187	6	9	0.61	0.21	31
Pd_2Pt_1	30.0	1/1	3.8966	3.9211	4	2	0.12	0.06	19
Pure Pt	8.0	–	3.9811		–	–	~0	–	–
Pd_4Au_1[d]	6.0	3.6/1	–	–	–	–	1.70	0.59	52

[a] All experiments were carried out in the solution of HCl (0.12 M)-ethanol by a tri-phase semibatch reactor at 10 °C, atmospheric pressure, and 5-h reaction. A trace amount of Pd and no Pt were leached from the silica surface to liquid as analyzed by ICP.
[b] The 3.3 wt.% of Pd was fixed for Pd alone and Pd–Pt/Au alloy catalysts, the subscripts are the molar ratios of Pd/Pt/Au in the bulk.
[c] The average particle size was obtained by TEM.
[d] Data taken from Ref. [13].
[e] Cell constants were obtained from XRD results analyzed using the Rietveld method.

sites. Comparing to the pure Pd catalyst, the catalyst performance was significantly improved upon alloying with the appropriate amount of Pt. In particular, the rate for H_2O_2 formation was 0.99 mol h^{-1} g_{Pd}^{-1} for pure Pd, and increased to 1.62 mol h^{-1} g_{Pd}^{-1} for Pd_8Pt_1 surpassed the maxima 1.77 mol h^{-1} g_{Pd}^{-1} for $Pd_{16}Pt_1$, then dropped down to 0.12 mol h^{-1} g_{Pd}^{-1} for Pd_2Pt_1. At the same time, the H_2O_2 selectivity increased from 12% for pure Pd to 70% for $Pd_{20}Pt_1$ and then went down to 19% for Pd_2Pt_1. Nevertheless, the selectivity of 70% for $Pd_{20}Pt_1$ is slightly lower than that (80%) obtained for a Pd/C catalyst under the similar reaction conditions as recently reported by Liu et al. [4]. It is noted that the performance for $Pd_{20}Pt_1$ is also superior to Pd_4Au_1 (Table 1) that was the best Pd-Au alloy catalyst we have ever prepared.

In addition, H_2O_2 decomposition, as a reverse reaction of H_2O_2 formation, was investigated with a solution of 1.0 wt.% H_2O_2 in a H_2 flow. As shown in Fig. 7, the activity order was displayed as $Pt \gg Pd_2Pt_1 > Pd_4Pt_1 > Pd_8Pt_1 > Pd_{16}Pt_1 \approx Pd_{20}Pt_1 \approx Pd$, being contrary to that for H_2O_2 synthesis.

4. Discussion

In line with previous studies [1,2], three competitive reactions [2] depicted as a triangular network (Scheme 1) were proposed to be mainly responsible for the production of H_2O_2 (reaction I) and H_2O (reaction II, III) in the direct reaction system. In addition, this reaction has been reported to be affected by several factors, such as halide ions, acid concentration, reaction medium, and catalyst property [1,2,5]. In order not to diverse the focus, herein, we mainly discuss the structure–activity relationship of this reaction system, the role of Pt, and the elementary steps involving the production of H_2O_2 and H_2O.

4.1. Structure of Pd–Pt alloys

The relationships of structure–activity of Pd–Pt alloy catalysts have been studied for several decades because of its important applications in electrochemistry, hydrogenation, and oxygen reduction reactions [10,24–29]. Generally, upon alloying with Pt, the Pd surface structure is modified through two ways: (i) the Pd ensembles in the surface are finely tuned by the change of the Pd–Pd bond length and (ii) the electronic density in the Pd valence band is changed by neighboring Pt atoms. In principle, Pd–Pt alloys are composed of continuously solid solutions, in which Pd and Pt atoms should be randomly mixed because of its relatively low enthalpy, for instance, only −4 kJ mol^{-1} for the formation of $Pd_{0.5}Pt_{0.5}$ [42]. However, theoretical studies [43–45] have evidenced that a strong segregation of Pd atoms may take place easily in the (1 0 0) and (1 1 1) surfaces of Pd–Pt alloys because of the lower surface energy of Pd and the greater cohesive energy of Pt. It has been further pointed out that for non-stoichiometric Pt–Pd clusters, even doping a single Pt atom into a Pd cluster (or vice versa) is sufficient to change the geometrical structure of the cluster [43]. The geometric structure and disorder degree for Pd–Pt nanoalloys were found to vary with the compositions of alloys [44].

In this study, the formation of alloys in the broad range of Pd/Pt ratios was demonstrated by the XRD patterns (Fig. 1). However, the Pd and Pt atoms in the bulks of alloys were not mixed homogenously because Pd-rich and Pt-rich mixed phases were detected for both Pd_4Pt_1 and Pd_2Pt_1 samples; meanwhile, the lattice constants (Table 1) varying between 3.9811 Å (pure Pt) and 3.8896 Å (pure Pd) reflect a contraction of Pt–Pt bond and an increase in the Pd–Pd distance in alloys [35]. On the other hand, the alloy surfaces were enriched by Pt as evidenced by XPS analysis (Fig. 3 and Table 1), this is contrary to the results reported by other groups [43,44]. A possible reason is that the effect of d-band filling may drive a segregation of the more electronegative Pt toward the surfaces [33].

The DRIFT spectra of CO adsorption (Fig. 4) showed an upshift of the linear CO–Pd band for Pd–Pt alloys, which is probably due to electron transfer from Pd to Pt. More interestingly, upon alloying with Pd, the linear CO–Pt band (2062 cm^{-1}) that could be observed for pure Pt disappeared completely accompanying with a significant decrease in the intensity of the bridge CO–Pd bands. In combination of all results, herein, two structure models for Pd–Pt nanoalloys [46] envisaged were depicted in Scheme 2. One is a Pd_{shell}–Pt_{core} model ((a) in Scheme 2), in which most of Pt atoms are located inside the bulk of nanoparticles. It may explain well that no linear CO–Pt band can be observed for alloy samples; however, it is contradictory with the fact of the Pt enrichment in alloy surfaces as detected by XPS. The other is a random model ((b) in Scheme 2), in which Pd and Pt are randomly distributed, and both atoms in the alloy surfaces are separated because of strong interactions. Likewise, it is understandable that the intensities for the bridge CO–Pd bands (Fig. 4) decrease drastically upon alloying with Pt, because the Pd atoms in alloy surfaces are highly diluted in comparison with that for pure Pd. The same reason may be responsible for the disappearance of the linear CO–Pt band on alloys, even

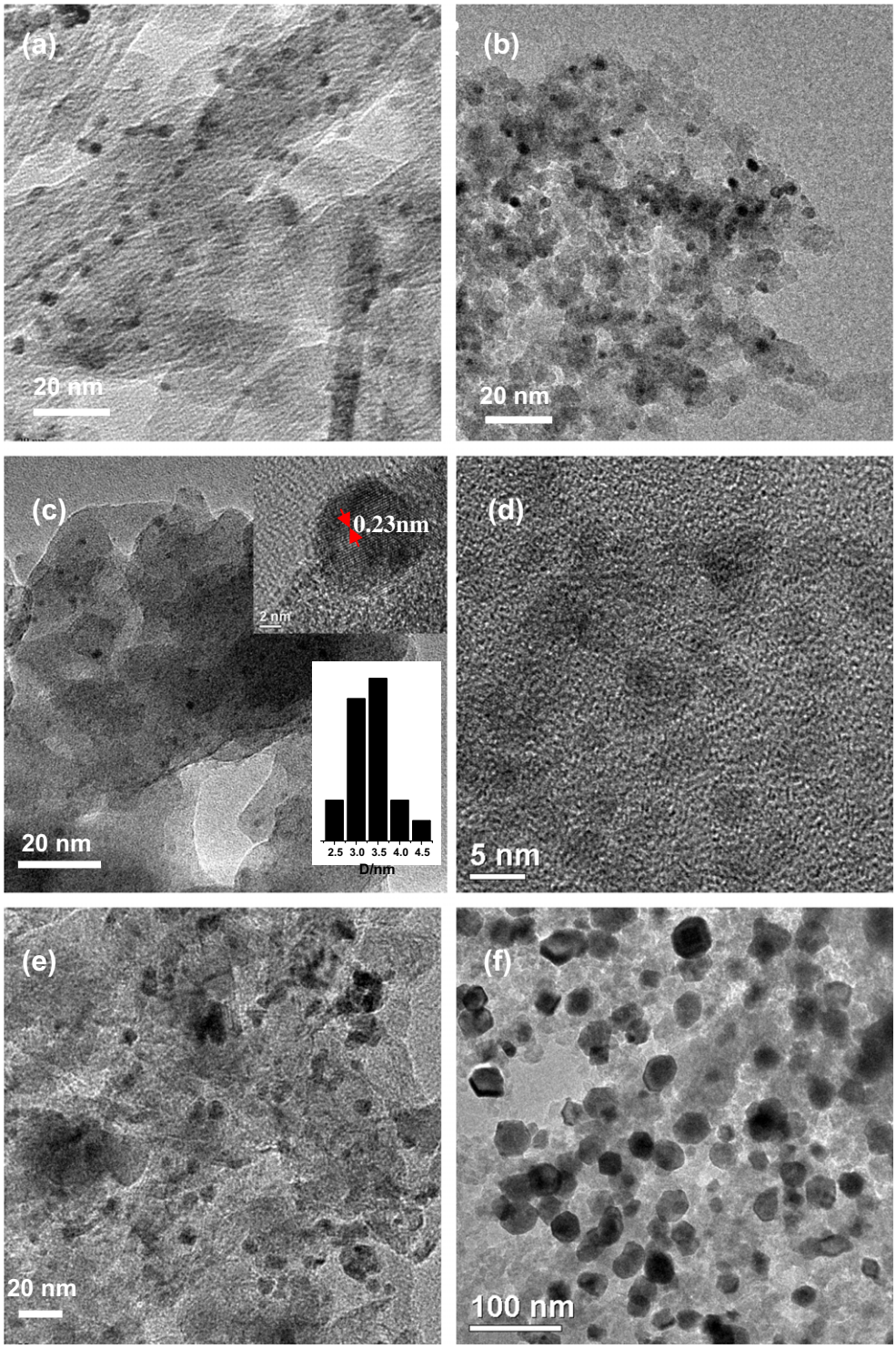

Fig. 2. TEM images of the fresh reduced catalysts. (a) Pure Pd, (b) $Pd_{20}Pt_1$, (c) $Pd_{16}Pt_1$, (d) Pd_8Pt_1, (e) Pd_4Pt_1, (f) Pd_2Pt_1.

though the Pt concentrations in the alloy surfaces are proved to be higher than those in the bulks. Owing to structure changes in nano-alloys, the capability of H_2 and O_2 adsorption on alloys was decreased drastically with increase in Pt concentration (Figs. 5 and 6).

4.2. Plausible mechanism

On the basis of the presented results, together with the previous studies [1,2,10], we assume that the mechanism for H_2O_2 synthesis on Pd–Pt alloy catalysts altered significantly compared to that on pure Pd. Elementary steps of this reaction were profoundly impacted during reaction, including the adsorption of H_2 and O_2, the formation and desorption of H_2O_2, and the decomposition of H_2O_2.

In the present reaction system, as illustrated in Scheme 1, side reactions such as H_2 over-oxidation and H_2O_2 decomposition occur simultaneously. Several elementary steps have been proposed for those reactions [10], as expressed by Eqs. (3)–(13):

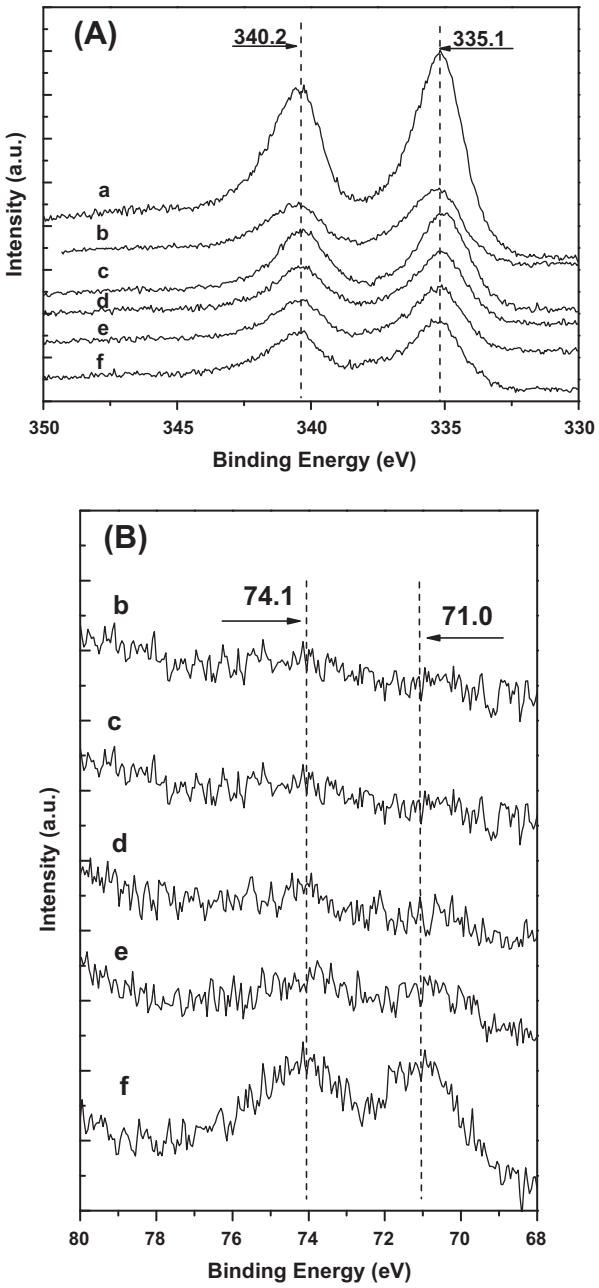

Fig. 3. (A) XPS Pd_{3d} spectroscopy and (B) XPS Pt_{4f} spectroscopy over the fresh reduced catalysts. (a) Pure Pd, (b) $Pd_{20}Pt_1$, (c) $Pd_{16}Pt_1$, (d) Pd_8Pt_1, (e) Pd_4Pt_1, (f) Pd_2Pt_1.

$$H_2(gas) \rightarrow H_{2ad} \quad (3)$$
$$O_2(gas) \rightarrow O_{2ad} \quad (4)$$
$$H_{2ad} \rightarrow 2H \quad (5)$$
$$O_{2ad} \rightarrow 2O \quad (6)$$
$$O_{2ad} + H \rightarrow OOH_{ad} \quad (7)$$
$$O + H \rightarrow OH_{ad} \quad (8)$$
$$OOH_{ad} + H \rightarrow H_2O_2 \quad (9)$$
$$OOH_{ad} + H_2 \rightarrow H_2O_2 + H \quad (10)$$
$$OH_{ad} + H \rightarrow H_2O \quad (11)$$
$$OH_{ad} + H_2 \rightarrow H_2O + H \quad (12)$$
$$H_2O_2 \rightarrow H_2O_2(gas) \quad (13)$$

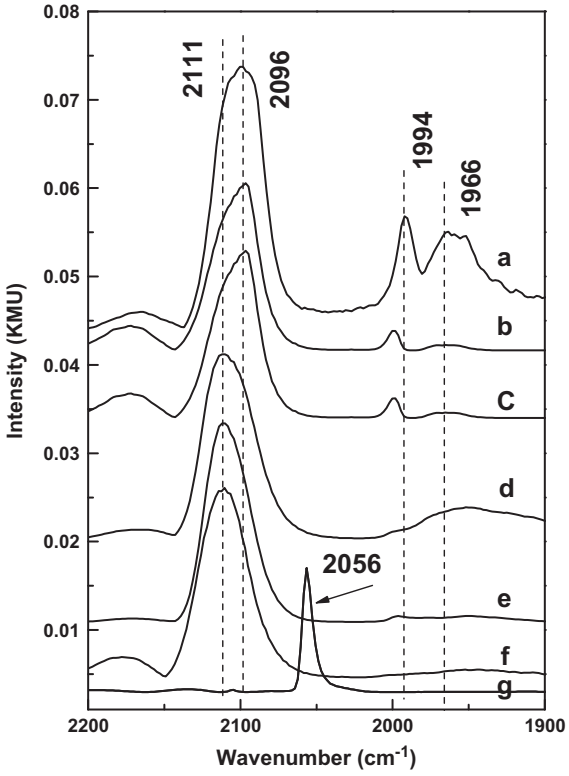

Fig. 4. In situ DRIFTS of CO (2.0% in He) adsorption. (a) Pure Pd, (b) $Pd_{20}Pt_1$, (c) $Pd_{16}Pt_1$, (d) Pd_8Pt_1, (e) Pd_4Pt_1, (f) Pd_2Pt_1, (g) pure Pt.

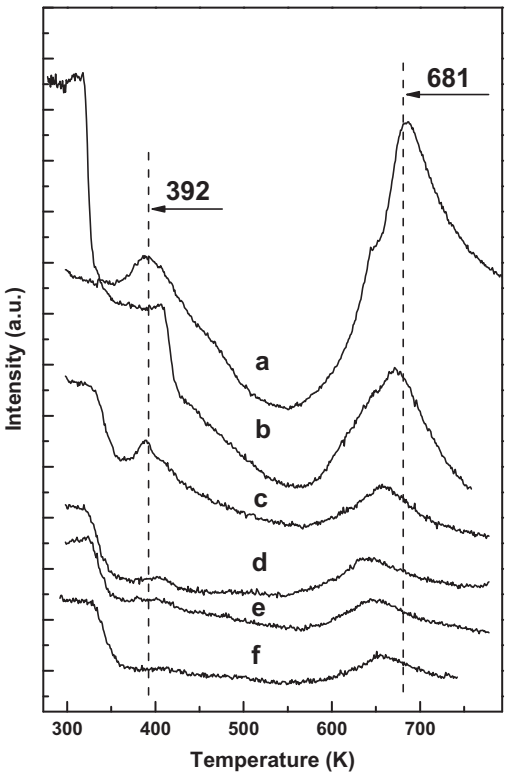

Fig. 5. H_2-TPD spectra. (a) Pure Pd, (b) $Pd_{20}Pt_1$, (c) $Pd_{16}Pt_1$, (d) Pd_8Pt_1, (e) Pd_4Pt_1, (f) Pd_2Pt_1.

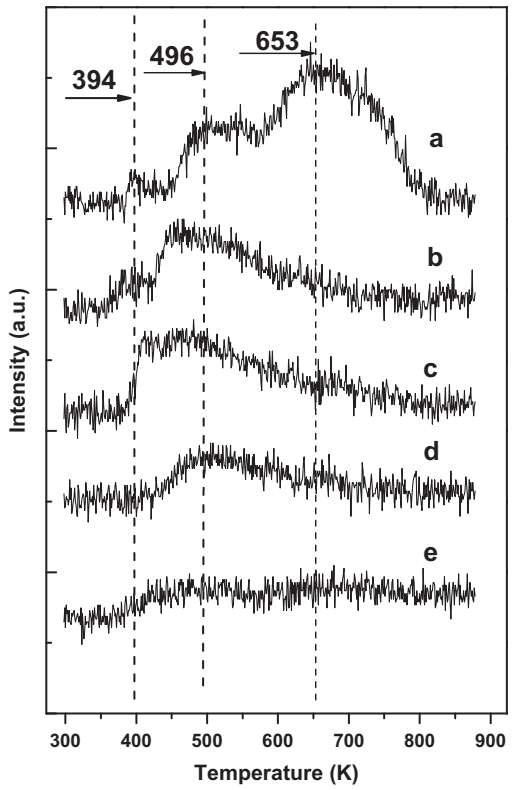

Fig. 6. O_2-TPD spectra. (a) Pure Pd, (b) $Pd_{20}Pt_1$, (c) $Pd_{16}Pt_1$, (d) Pd_8Pt_1, (e) Pd_2Pt_1.

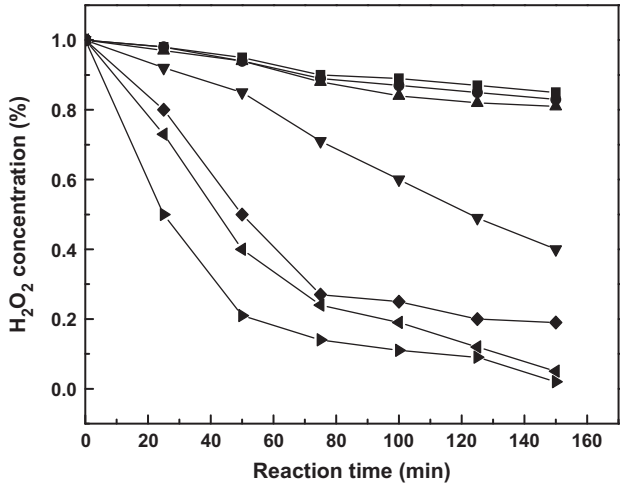

Fig. 7. Decomposition of H_2O_2 over all catalysts, pure Pd (■), $Pd_{20}Pt_1$(●), $Pd_{16}Pt_1$ (▲), Pd_8Pt_1 (▼), Pd_4Pt_1(♦), Pd_2Pt_1(◄), pure Pt (►). Reaction conditions: initial 1.0 wt.% H_2O_2 in ethanol (90 mL) + water (10 mL), 0.12 N HCl, 283 K, H_2 flow rate of 15 mL/min.

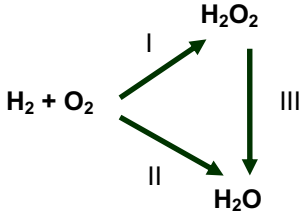

Scheme 1. Reaction network in the synthesis of H_2O_2: (I) formation of H_2O_2; (II) formation of H_2O by H_2 oxidation; (III) formation of H_2O by H_2O_2 decomposition.

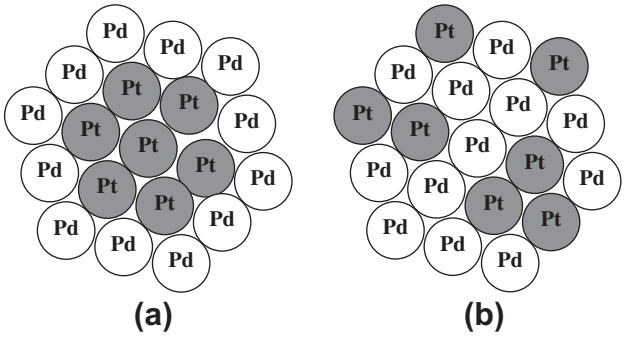

Scheme 2. Cross-section of the Pd–Pt nanoparticle models: (a) Pd_{shell}–Pt_{core}; (b) random model [44].

Gaseous O_2 and H_2 molecules were first adsorbed on active sites (Eqs. (3) and (4)) and then dissociated into atomic O and H immediately (Eqs. (5) and (6)). It has been demonstrated that molecular O_2 and H_2 can dissociate readily at 120 K [47] and 40 K [48] on the Pd(1 1 1) surface. Furthermore, parts of O_2 molecules that were probably weakly bonded to the Pd atoms were reacted with H to produce OOH_{ad} (Eq. (7)), while the O and H atoms reacted with each other to form OH_{ad} (Eq. (8)). OOH_{ad} and $OH^{\cdot}_{ad}$ are believed to be the primary intermediates involved into reactions for the production of H_2O_2 and H_2O, respectively. In particular, H_2O_2 was probably generated through the interaction between OOH_{ad} and atomic (Eq. (9)) or molecular hydrogen on the Pd surface (Eq. (10)). However, we argue the reaction of Eq. (10) unlikely occurs because of the low diffusion rate of H_2 from gas phase to the catalyst surface [2]. On the other hand, OH_{ad} also reacted with atomic (Eq. (11)) and molecular (Eq. (12)) hydrogen to generate H_2O. Finally, H_2O_2 was desorbed from metal surfaces (Eq. (13)). It is worthy to note that other pathways for H_2O_2 formation such as $OH^{\cdot}$ radical disproportionation suggested by Olivera et al. [10] are not displayed here because those reactions are kinetically unfavorable.

The Lunsford's group has proposed that the colloidal palladium derived either from Pd/SiO_2 or from $PdCl_2$ via the reduction in $PdCl_4^{2-}$ ions in aqueous solutions acidified by HCl may work as active sites for H_2O_2 synthesis [2,4,7,21,22]. However, in the present system, the Pd^{2+} concentration in the working solution was below 3 ppm after reaction of 5 h, suggesting that only a trace amount of Pd was leached during reaction. Therefore, we assume that H_2O_2 is produced mainly on the solid catalyst surface.

4.3. The Pt role

Up to date, little experimental evidence has been found for the proposed reaction mechanisms because of technical limitations. $OOH^{\cdot}$ radical is believed to be the primary intermediate species in the generation of H_2O_2 (Eqs. (9) and (10)) [2,49]. Dissanayake and Lunsford have investigated the dissociative adsorption of oxygen on a Pd/SiO_2 catalyst during reaction using a mixture of $^{16}O_2$ and $^{18}O_2$ [21,22]. $H_2{}^{16}O^{18}O$, as a major product, should be detected whether a dissociated form of oxygen were involved. However, as evidenced by the Raman spectra, only $H_2{}^{16}O_2$ with a peak at 879 cm^{-1} and $H_2{}^{18}O_2$ with a peak at 830 cm^{-1} were present as products. Meanwhile, no significant peak was detected at about 852 cm^{-1}, which corresponds to $H_2{}^{16}O^{18}O$. Clearly, H_2O_2 is derived only from a diatomic form of oxygen that is presumably adsorbed on the Pd sites.

The addition of a small amount of Pt into Pd phase (from Pd to $Pd_{16}Pt_1$) could significantly enhance H_2O_2 synthesis (Table 1). It can be explained that the dissociative adsorption of oxygen on the alloy surfaces (Eq. (6)) may be suppressed by the weakening

of Pd–O bonds, which will lead to an increase in the concentration of OOH· radicals (Eq. (7)) and the reaction rate of Eq. (9). In short, the formation of OH· radicals, which is the only intermediate responsible for H_2O synthesis, was greatly reduced. Obviously, the Pt role in Pd–Pt alloy catalysts is different from the Au role in Pd–Au alloy catalysts, in which synergetic effects of Au and Pd on the adsorption and transfer of oxygen were suggested [13].

The excess Pt atoms in alloys (Pd/Pt < 8) led to a drastic decrease in the production of H_2O_2 (Table 1). This fact may be explained with the following reasons: (i) the high coverage of Pt on the Pd surface blocks the adsorption of reactants on the Pd sites, as evidenced by the O_2/H_2-TPD experiments (Figs. 5 and 6); (ii) the kinetics of oxygen dissociation may be favored on the higher Pt content catalysts, and theoretical studies [10,36] revealed the bond strength of oxygenated species such as OOH· radical on the Pt sites was stronger than that on the Pd sites, while O and OH· could be reduced to H_2O on the Pt sites; (iii) H_2O_2 tends to dissociate on the Pt sites. Actually, H_2O_2 is prone to decompose on all catalysts during reaction (Fig. 7) as depicted in Eqs. (14) and (15) [2]. The rate for H_2O_2 decomposition was almost unaffected by Pt from pure Pd to $Pd_{16}Pt_1$, but enhanced significantly with continuous increase in the Pt content. The excess Pt atoms may facilitate H_2O formation because of reasons (ii) and (iii). It is also understandable that pure Pt is incapable of generating H_2O_2 but H_2O.

$$H_2O_2 \rightarrow H_2O + 1/2O_2 \quad (14)$$

$$H_2O_2 + H_2 \rightarrow 2H_2O \quad (15)$$

A common point is that the rate for H_2O_2 formation is dependent on the surface hydrogen coverage, which is affected by H_2 diffusion from liquid to solid catalyst surfaces [2]. It seems to be contradictory to the phenomenon observed from the H_2-TPD spectra, which has proven the adsorption amount of H_2 is irrelevant with H_2O_2 formation. As listed in Table 1, an increase in Pt concentration in alloys caused a remarkable decrease in the capability for H_2 adsorption but enhancing the activity. For example, the desorption amount of H_2 dropped drastically from 106 (pure Pd) to 7 (Pd_8Pt_1) $\mu mol/g_{cat}$ corresponding to the rate of 0.99 and 1.62 mol/h g_{Pd}, respectively. This fact suggests that the surface hydrogen coverage is not a decisive factor for H_2O_2 formation.

Furthermore, the surface structures of the catalysts may be modified further during reaction because of adsorption and reaction-induced reconstructions. The reasons for the Pt promotional effects could be more complex than we have speculated here, and several questions about the mechanism have still no clear-cut answers. For instance, how is the surface local structure changed owing to the addition of Pt? Whether the charge transfer between Pd and Pt impacts on the adsorption and stabilization of the adsorbed molecular O_2 and its subsequent reactions with hydrogen. The relevant study is still ongoing in our laboratory.

5. Conclusions

H_2O_2 synthesis could be improved greatly over the Pd catalysts upon alloying with Pt. Among all catalysts, $Pd_{16}Pt_1$ showed the best performance with a rate of 1.77 mol h^{-1} g_{Pd}^{-1} and a selectivity of 60%, while 0.99 mol h^{-1} g_{Pd}^{-1} and only 12% observed for pure Pd. Excess Pt (Pd/Pt < 8) in alloys could remarkably deteriorate the catalytic performance.

As evidenced by the XRD results, alloys were created in the whole Pd/Pt ratio range, and two separated alloy phases (Pd-rich and Pt-rich Pd–Pt alloys) were observed for Pd_4Pt_1 and Pd_2Pt_1, respectively. In situ DRIFTS of CO adsorption and XPS results have proved that the Pd–Pt alloy surfaces were enriched by Pt. The changes in the surface structures may be responsible for the decline of the adsorption capability to H_2 and O_2, as evidenced by the spectra of O_2-TPD and H_2-TPD.

We speculate that the tuning of Pd electronic structure by the addition of a small amount of Pt may stabilize dioxygen on the Pd sites, which is the precursor for the formation of OOH· radicals that react with atomic and molecular hydrogen to form H_2O_2. However, excess Pt may destabilize OOH· radicals and decompose H_2O_2 into H_2O.

Acknowledgments

The authors are grateful to the support from the Chinese Education Ministry 111 Project (B08021), the National Science Foundation (21176071, 21106041), Shanghai PuJiang Talent Program (2010/10PJ1402500, 2011/11PJ1402400), Innovation Program of Shanghai Municipal Education Commission (11ZZ52), Shanghai Natural Science Foundation (11ZR1408400), Opening Project Program of State Key Laboratory of Chemical Engineering (SKL-ChE-10C05), Creative Team Development Project of Ministry of Education (IRT0721), and Fundamental Research Funds for the Central Universities.

References

[1] J.M. Campos-Martin, G. Blanco-Brieva, J.L.G. Fierro, Angew. Chem. Int. Ed. 45 (2006) 6962.
[2] J.H. Lunsford, J. Catal. 216 (2003) 455.
[3] W.T. Hess, in: J.I. Kroschwitz, M. Howe-Grant (Eds.), Kirk–Othmer Encyclopedia of Chemical Technology, fourth ed., vol. 13, Wiley, New York, 1995, p. 961.
[4] Q. Liu, J.C. Bauer, R.E. Schaak, J.H. Lunsford, Angew. Chem. Int. Ed. 47 (2008) 1.
[5] Y.-F. Han, J.H. Lunsford, J. Catal. 230 (2005) 313.
[6] V.R. Choudhary, P. Jana, J. Catal. 246 (2007) 434.
[7] Y.-F. Han, J.H. Lunsford, Catal. Lett. 99 (2005) 13.
[8] R.E. Schaak, A.K. Sra, B.M. Leonard, R.E. Cable, J.C. Bauer, Y.-F. Han, J. Means, W. Teizer, Y. Vasquez, E.S. Funck, J. Am. Chem. Soc. 127 (2005) 3506.
[9] Q. Chen, E.J. Beckman, Green Chem. 9 (2007) 802.
[10] P.P. Olivera, E.M. Patrito, H. Sellers, Surf. Sci. 313 (1994) 25.
[11] S. Abate, G. Centi, S. Perathoner, S. Melada, F. Pinna, G. Strukul, Topics Catal. 38 (2006) 181.
[12] S. Melada, F. Pinna, G. Strukul, S. Perathoner, G. Centi, J. Catal. 237 (2006) 213.
[13] Y.-F. Han, Z. Zhong, K. Ramesh, F. Chen, L. Chen, T. White, Q. Tay, S.N. Yaakub, Z. Wang, J. Phys. Chem. C 111 (2007) 8410.
[14] L.W. Gosser, Jo-Ann T. Schwartz, US Patent 4832938, to E. I. Du Pont de Nemours and Company, 1989.
[15] Q. Liu, J.C. Bauer, R.E. Schaak, J.H. Lunsford, Appl. Catal. A: Gen. 339 (2008) 130.
[16] J.K. Edwards, B.E. Solsona, P. Landon, A.F. Carley, A. Herzing, C.J. Kiely, G.J. Hutchings, J. Catal. 236 (2005) 69.
[17] P. Landon, P.J. Collier, A.F. Carley, D. Chadwick, A.J. Papworth, A. Burrows, C.J. Kiely, G.J. Hutchings, Phys. Chem. Chem. Phys. 5 (2003) 1917.
[18] J.K. Edwards, B. Solsona, E. Ntainjua N, A.F. Carley, A.A. Herzing, C.J. Kiely, G.J. Hutchings, Science 323 (2009) 1037.
[19] V.V. Krishnan, A.G. Dokoutchaev, M.E. Thompson, J. Catal. 196 (2000) 366.
[20] T.A. Pospelova, N.I. Kobozev, E.N. Ermin, Rus. J. Phys. Chem. (Trans) 35 (1961) 143.
[21] D.P. Dissanayake, J.H. Lunsford, J. Catal. 206 (2002) 173.
[22] D.P. Dissanayake, J.H. Lunsford, J. Catal. 214 (2003) 113.
[23] C. Burato, S. Campestrini, Y.-F. Han, P. Canton, P. Centomo, P. Canu, B. Corain, Appl. Catal. A. 358 (2009) 224.
[24] K. Persson, K. Jansson, S.G. Järås, J. Catal. 245 (2007) 401.
[25] R. Strobel, J.-D. Grunwaldt, A. Camenzind, S.E. Pratsinis, A. Baiker, Catal. Lett. 104 (2005) 9.
[26] P.B. Balbuena, S.R. Calvo, E.J. Lamas, P.F. Salazar, J.M. Seminario, J. Phys. Chem. B 110 (2006) 17452.
[27] J.R. Chang, S.L. Chang, T.B. Lin, J. Catal. 169 (1997) 338.
[28] A. Stanislaus, B.H. Cooper, Catal. Rev. Sci. Eng. 36 (1994) 75.
[29] R. Ferrando, J. Jellinek, R.L. Johnston, Chem. Rev. 108 (2008) 845.
[30] Y.-F. Han, D. Kumar, D.W. Goodman, J. Catal. 230 (2005) 353.
[31] H.W. King, F.D. Manchester, J. Phys. F 8 (1978) 15.
[32] J.F. Moulder, W.F. Stickle, P.E. Sobol, K.D. Bomben, in: J. Chastain, C. King Jr. (Eds.), Handbook of X-ray Photoelectron Spectroscopy, Physical Electronics, Inc., 1995. ISBN: 0-9648124-1-X.
[33] A. Dianat, J. Zimmermann, N. Seriani, M. Bobeth, W. Pompe, L.C. Ciacchi, Surf. Sci. 602 (2008) 876.
[34] R.R. Squires, J. Am. Chem. Soc. 107 (1985) 4385.
[35] S.R. Calvo, P.B. Balbuena, Surf. Sci. 601 (2007) 4786.
[36] M. Lepage, T. Visser, Ad M.J. van der Eerden, F. Soulimani, B.M. Weckhuysen, Vib. Spectrosc. 48 (2008) 92.
[37] O. Alexeev, D.-W. Kim, G.W. Graham, M. Shelef, B.C. Gates, J. Catal. 185 (1999) 170.

[38] T. Rades, V.Yu. Borovkov, V.B. Kazansky, M. Polisset-Thfoin, J. Fraissard, J. Phys. Chem. 100 (1996) 16238.
[39] Y. Wang, N. Toshima, J. Phys. Chem. B 101 (1997) 5301.
[40] N.V. Hieu, J.H. Craig Jr., Surf. Sci. 150 (1985) L93.
[41] H.H. Kan, R.B. Shumbera, J.F. Weaver, Surf. Sci. 602 (2008) 1337.
[42] F.R. De Boer, R. Boom, W.C.M. Mattens, A.R. Miedama, A.K. Niessen, Cohesion in Metals: Transition Metal Alloys, Elsevier, Amsterdam, 1988.
[43] C. Massen, T.V. Mortimer-Jones, R.L. Johnston, J. Chem. Soc., Dalton Trans. 23 (2002) 4375.
[44] L.D. Lloyd, R.L. Johnston, S. Salhi, N.T. Wilson, J. Mater. Chem. 14 (2004) 1691.
[45] D.J. Watson, G.A. Attard, Surf. Sci. 515 (2002) 87.
[46] N. Toshima, M. Harada, T. Yonezawa, K. Kushihashi, K. Asakura, J. Phys. Chem. 95 (1991) 7448.
[47] M.K. Rose, A. Borg, J.C. Dunphy, T. Mitsui, D.F. Ogletree, M. Salmeron, Surf. Sci. 561 (2004) 69.
[48] H. Conrad, G. Ertl, E.E. Latta, Surf. Sci. 41 (1974) 435.
[49] T.A. Pospelova, N.I. Kobozev, Rus. J. Phys. Chem. (Trans.) 35 (1961) 262.